Stress-driven buckling patterns in spheroidal core/shell structures

Jie Yin[a], Zexian Cao[b], Chaorong Li[c], Izhak Sheinman[a,d], and Xi Chen[a,1]

[a]Department of Civil Engineering and Engineering Mechanics, Columbia University, New York, NY 10027-6699; [b]Institute of Physics, Chinese Academy of Sciences, P.O. Box 603, Beijing 100190, China; [c]Department of Physics and Key Laboratory of Advanced Textile Materials and Manufacturing Technology, Zhejiang Sci-Tech University, Hangzhou 310018, China; and [d]Faculty of Civil and Environmental Engineering, Technion-Israel Institute of Technology, Haifa 32000, Israel

Many natural fruits and vegetables adopt an approximately spheroidal shape and are characterized by their distinct undulating topologies. We demonstrate that various global pattern features can be reproduced by anisotropic stress-driven buckles on spheroidal core/shell systems, which implies that the relevant mechanical forces might provide a template underpinning the topological conformation in some fruits and plants. Three dimensionless parameters, the ratio of effective size/thickness, the ratio of equatorial/polar radii, and the ratio of core/shell moduli, primarily govern the initiation and formation of the patterns. A distinct morphological feature occurs only when these parameters fall within certain ranges: In a prolate spheroid, reticular buckles take over longitudinal ridged patterns when one or more parameters become large. Our results demonstrate that some universal features of fruit/vegetable patterns (e.g., those observed in Korean melons, silk gourds, ribbed pumpkins, striped cavern tomatoes, and cantaloupes, etc.) may be related to the spontaneous buckling from mechanical perspectives, although the more complex biological or biochemical processes are involved at deep levels.

morphogenesis | nonlinear mechanics | pattern formation | physical geometry

Spontaneous buckling of thin films on compliant substrates can achieve numerous highly ordered patterns due to mismatched deformation (1–6), which can be manipulated in different ways (1, 7–9). Buckling may also play an important role in the morphogenesis of some plant parts, including phyllotactic pattern in compressed tunica (10, 11), primordium initiation in sunflower capitulum (12), and Fibonacci patterns resembling those in some flowering cactus and pine cones (2), among others, in a way that is similar to the energy-minimizing buckling of a compressed shell on an elastic foundation (10).

Many natural fruits and vegetables can be approximated as spheroidal stiff exocarp (shell)/compliant sarcocarp (core) systems, which exhibit intriguing buckle-like profiles. For example, the Korean melon (yellow melon) and ridged gourd (or silk gourd, *luffa acutangula*) are distinguishable by 10 equidistant longitudinal ridges that run from stem to tip. Small pumpkins, acorn squashes, and carnival squashes often have ~10 uniformly spaced ribs, whereas the large pumpkins often have ~20 or more ridges. Similar undulating morphologies found in varieties of cucumis melons, gourds, striped cavern tomatoes, bell peppers, and other fruits and vegetables underpin their distinctive appearances. Although pattern formation in plants usually involves various complex biological and biochemical processes (11, 13, 14), such distinctive yet simple features make one wonder whether there exist other relatively simpler mechanisms contributing to the morphogenesis at the macroscopic scale, and the possibility of stress-driven buckling is explored in this study.

Consider a model spheroidal core/shell system where the shell is characterized by $(x^2 + y^2)/a^2 + z^2/b^2 = 1$ with equatorial radius a, polar radius b, and thickness t ($t \ll a$); the system remains closed and bonded together in the due course of buckling. Both film (shell) and substrate (core) are assumed to be homoge-

neous, isotropic and elastic, with their Young's moduli and Poisson's ratios denoted as E_f and v_f, and E_s and v_s, respectively ($E_f > E_s$). When the current model is applied to fruits and vegetables, the parameters (E_f, E_s, t) should be regarded as the "effective" (or nominal) variables because the true properties of fruit/vegetable components may be inhomogeneous, anisotropic, and gradient. We also neglect the boundary effect (e.g., the constraint imposed by the stem and the navel at a polar end) and assume no external constraint during the growth.* The simplified model system is used to reveal useful insights of the important parameters governing pattern formations.

The growth in plants can be analogously simulated (15) without any external guidance, and we assume that the unconstrained growth is isotropic and uniform within both film and substrate. Because the outer layer of plant meristems often expands faster than the inner one (12, 16), the growth expansion coefficient (rate) is larger in the shell than that of the core. The mismatch between the expansion of the stiff thin film and soft thick substrate causes the benign growth stress in the film compressive.

For a prolate spheroid ($k = b/a > 1$) or oblate spheroid ($k < 1$), the in-plane stress in the film is non-equi-biaxial (anisotropic) and increases with growth in the prebuckled state, where an interface pressure is acting on the film due to the expansion mismatch. Neglecting the shear stress at interface (9), the ratio between the prebuckling hoop (σ_h) and longitudinal (σ_l) growth stresses at any point in the spheroidal film is [see supporting information (SI) *Text*]

$$\sigma_h/\sigma_l = 2 - \cfrac{1}{1 + \cfrac{x_0^2}{R^2}\left(1 - \cfrac{1}{k^2}\right)} \qquad [1]$$

where x_0 is the radius of latitudinal circle and $R = a^2/b$ is the radius of curvature at the pole. Apparently, $\sigma_h/\sigma_l > 1$ in a prolate spheroid, whereas $\sigma_h/\sigma_l < 1$ in an oblate system; the stress ratio also depends on the size of spheroid. Denote $\sigma_f = \text{Max}(\sigma_h, \sigma_l)$, the film starts to buckle when $\sigma_f = \sigma_c$ and σ_c is a critical stress—above such critical stress level, various buckle patterns emerge depending on the geometrical and material constraints, and the undulations tend to relax the higher stress component. The spontaneous buckles are simulated by using the finite element method (FEM) (see *SI Text*).
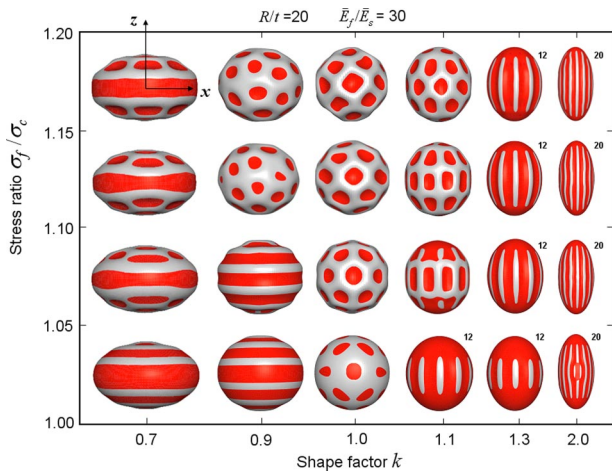

Fig. 1. Deformation map of spheroid as both parameter *k* and film stress are varied (with $R/t = 20$ and $\bar{E}_f/\bar{E}_s = 30$). In all buckled morphologies in Figs. 1–3 and Figs. S1 and S2, the dark (red) areas mean that within such concave regions, the magnitude of the radial displacement is smaller than a certain value; all snapshots of the morphology are rescaled to fit into the map. For ridged morphology, the number of buckles is shown on the top corner of each simulated pattern.

Results and Discussion

Four effective dimensionless parameters, the normalized size $R/t = a^2/bt$, the shape factor $k = b/a$, the modulus ratio $\bar{E}_f/\bar{E}_s = E_f(1 - \nu_s^2)/E_s(1 - \nu_f^2)$, and the normalized growth stress σ_f/σ_c, primarily affect the stress-driven buckling patterns. In Fig. 1, for representative values of $R/t = 20$ and $\bar{E}_f/\bar{E}_s = 30$, the buckled patterns vary with σ_f/σ_c and k (transition from oblate to prolate shape). When $k = 1.0$, according to Eq. 1, $\sigma_h/\sigma_l = 1$, and thus, reticular buckle patterns are formed on spherical core/shell system when R/t is not very large (17) and the buckle amplitude increases with σ_f/σ_c, as shown in Fig. 1. In spherical systems with large R/t, labyrinth undulations appear—the buckling mechanisms of spherical film/substrate systems have been studied in ref. 17.[†] Note that the stress field is also isotropic ($\sigma_h/\sigma_l = 1$) if the substrate is planar without further manipulation of system properties (e.g., anisotropic growth), and the resulting buckling patterns have no directional preference; the principles of pattern formations on planar substrates (under both isotropic and anisotropic stresses) have been discussed extensively in earlier works, e.g., refs. 8, 9, and 18–20. In the present article with the spheroidal substrate, the stress is anisotropic when $k \neq 1$, which leads to distinct buckling mechanisms and more variety of undulation morphologies than those on a spherical substrate (17), and they are explored in detail as well as their implications in fruit morphogenesis.

In the case of slight deviation from spherical shape, e.g., setting $k = 0.9$ and 1.1, ordered latitudinal and pumpkin-like ribbed patterns are formed at the onset of buckling, respectively, which then transit to triangular patterns at higher stresses. With the more evidently oblate or prolate spheroids, the buckling pattern persists with film growth. In particular, when k is larger than ~ 1.3, the hoop/longitudinal growth stress ratio σ_h/σ_l becomes increasingly ~ 1 and reaches its maximum at the equator; consequently, equidistant longitudinal buckle ribs are first formed near the equator and extend to the poles as σ_f/σ_c is increased.
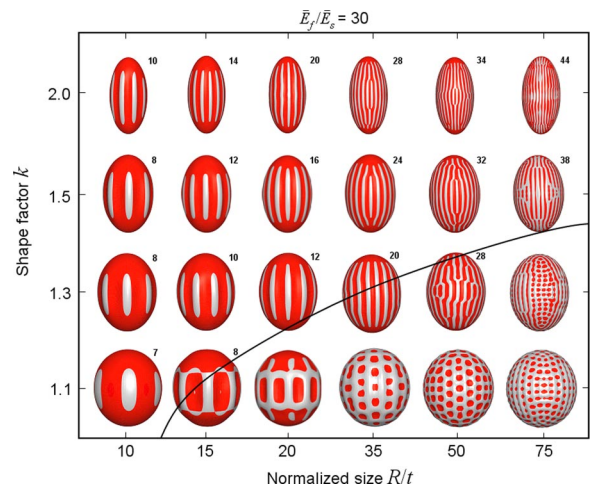
Fig. 2. Deformation map of a prolate spheroid with varying *k* and *R/t* (with $\bar{E}_f/\bar{E}_s = 30$). The black solid line separates the ribbed and reticular patterns (same for Fig. 3). The initial buckle patterns ($\sigma_f/\sigma_c \approx 1.05$) are shown.

Because most fruits and vegetables with undulating morphology are prolate (in an approximate sense), in the following we focus on the buckling in prolate spheroids (especially those with $k \geq 1.3$). With reference to Eq. 1, if R/t is very large, σ_h/σ_l decreases to approach the value of 1.0, consequently circumferential buckles may emerge (Fig. S1). At lower values of R/t ($R/t \leq 30$), the stress anisotropy is higher and the ribbed morphology remains quite robust with continued moderate level of shell growth, which can be confirmed when both $\bar{E}_f/\bar{E}_s$ and k are varied in a large range, Fig. S1 and Fig. S2 [if the growth strain is too large, the ridged morphology may become unstable (19)]. Owing to such a relative stability, we will explore subsequently how the initial buckle pattern ($\sigma_f/\sigma_c \approx 1.05$) varies with the 3 dimensionless ratios (k, R/t, $\bar{E}_f/\bar{E}_s$).

In the first buckling map (Fig. 2), $\bar{E}_f/\bar{E}_s = 30$ while k and R/t are varied. The solid line is a rough boundary to distinguish the geometrical parameter space of longitudinal ridged patterns from that of reticular ones. When k is fixed, with the increase of R/t (i.e., the larger a/t), the number of longitudinal ribs grows rapidly in accompany with the occurrence of circumferential waves, and the buckle finally transits to a reticular pattern at large R/t. Governed by the competition between k and R/t on growth stress (Eq. (1)), the longitudinal ridged buckle takes over at larger k and/or smaller R/t; otherwise the addition of circumferential waves makes the buckles reticular. At constant R/t, with the increase of k the ridged buckle dominates and the ridge number also increases primarily due to the increase of a/t. In such longitudinal ridged patterns the number of ribs is essentially only a function of a/t and $\bar{E}_f/\bar{E}_s$, as will be discussed below.

For a representative $k = 1.3$, the buckling map in Fig. 3 shows that at a fixed geometrical factor (R/t), the wave length of the buckled ridges increases with the elastic mismatch. At small $\bar{E}_f/\bar{E}_s$ and large R/t, reticular pattern ensues; otherwise, ribs prevail which may extend to the polar regions as R/t increases. Near the boundary (solid line), one could identify the upper limits of the ribs in the stable longitudinal ridged configuration. When R/t is relatively small, the wave number appears to be quite stable against a large variation of $\bar{E}_f/\bar{E}_s$.

At large k, the prolate spheroid may be approximated as a long cylinder of radius a. The buckle wave number can be estimated as:

$$n_{cr} \approx \left(\frac{a}{t}\right)^{\frac{3}{4}}\left(\frac{12\tilde{E}_s}{\bar{E}_f}\right)^{\frac{1}{4}} \qquad [2]$$

Fig. 3. Deformation map of a prolate spheroid with varying $\bar{E}_f/\bar{E}_s$ and R/t (with $k = 1.3$). The initial undulation patterns ($\sigma_f/\sigma_c \approx 1.05$) are shown.

where $\bar{E}_s = E_s/(1 + v_s)(1 - 2v_s)$ (see *SI Text*). Even at a relatively small k, $k = 1.3$ say, the wave number predicted by Eq. **2** is reasonably close to that obtained from FEM simulations of prolate spheroids (Fig. S3); the small difference is due to the geometrical constraints at capped poles and also to the system instability at large R/t. Hence, the characteristics of longitudinal ridged pattern is dominated by a/t (substrate curvature) and $\bar{E}_f/\bar{E}_s$ (film/substrate modulus mismatch) and more ribs are possible with larger a/t and/or smaller $\bar{E}_f/\bar{E}_s$, as validated from Figs. 2–3.

Despite the complicated cellular processes involved during the growth of some fruits and plants, mechanical buckling may reproduce similar ribbed and reticular morphologies for prolate spheroidal core/shell structures (Fig. 4). The results demonstrate that a distinct profile is possible only when the 3 geometrical and material parameters fall within a certain range. For example, examination of the Korean melon shows that its effective R/t is ~15–18, and k is ~1.2–1.4, which may justify its 10 equidistant longitudinal ridges (see Fig. 2); in addition, to maintain such a profile, the effective $\bar{E}_f/\bar{E}_s$ may vary between ~20 and 40 (see Fig. 3). Similarly, if the distinct patterns are related to buckling, for ridged gourd whose $k \approx 5$–6, its effective R/t and $\bar{E}_f/\bar{E}_s$ should be ~4–5 and 20–30, respectively; for striped cavern tomatoes with 4–6 ridged buckles, the effective R/t is ~5; and for reticular patterns to prevail, cantaloupes ($k \approx 1.1$–1.2) should have a large R/t and a low $\bar{E}_f/\bar{E}_s$. A resembler of pumpkins may be obtained by modifying the spheroid model (Fig. S4); because the wave

number is related to the normalized equatorial radius (a/t), Fig. 4 shows that in a small pumpkin simulant, 10 ridges may emerge, and when a/t grows larger, 20 or more ribs are possible. In all cases, the ridged patterns are also robust when the effective mismatch $\bar{E}_f/\bar{E}_s$ varies within a moderate range (Fig. 3); indeed, moderate variations of material properties are reasonable during fruit/vegetable growth (21) and despite the scatter of properties in individual fruits/vegetables, certain species (e.g., Korean melon) still exhibit a distinct topology.

There is no doubt that biological and biochemical processes also play a very important role in regulating the plant pattern formation. In leaf morphology for example, the mutation of CIN gene found in *Antirrhinum* exhibits excess growth in marginal regions (22), which makes the edges in compression and turns the normally flat leaves into wavy surfaces with buckled margins. Similar studies on *Arabidopsis* (23) and eggplant leaf (24) suggest a role for mechanical force in the regulation of plant morphology through its interaction with biological processes. The phenomenological study of stress-driven buckling in a spheroidal core/shell system may suggest a similar regulatory pathway: With the excessive growth of the shell-like exocarp (through certain biological processes), buckling occurs due to mechanical forces where the initiation locations and characteristics (e.g., the number of ribs) are roughly controlled by the aforementioned mechanical principles. Meanwhile, the effective material properties relevant to buckling modes are based on cellular properties of the exocarp and sarcocarp. During the buckling process, the mechanical forces may also confine and interact with certain biological processes such as cell growth and cell differentiation (11, 14) to help stabilize the global pattern features. In other words, the morphology of some plants/fruits may result from a concerted effort of the mechanical and biological processes.

We notice that the dehydration process or a fruit or vegetable can be free from the biological factors that could have been involved in its growth; therefore the surface pattern of a dehydrated fruit (or vegetable) is dominated by buckling. In a dried mini tomato (Fig. S5), the longitudinal ridges are analogous to that shown in Fig. 3 and the wave numbers are also associated with (k, R/t, and $\bar{E}_f/\bar{E}_s$) (the latter 2 factors are of more weight). In addition, experiments were carried out on a SiO_2 shell/Ag core microsystem, and the observed buckle patterns (Fig. S6) qualitatively agree with simulation (see *SI Text*); such results also demonstrate the potential applications in micro- and nanofabrications via controlled self-assembly on curved/closed substrate surfaces.

Conclusion

Although Charles Darwin remarked that the explanation of plant pattern formation could "drive the sanest man mad" (25), anisotropic stress-driven buckling in spheroidal core/shell system, as we

Fig. 4. Comparison between several fruits/vegetables and examples of corresponding simulated buckle shapes on model spheroids (see *SI Text* for more details).

Yin *et al.*

have shown here, could, to some extent, resemble the global pattern features formed in the appearance of quite many kinds of fruits and vegetables, and each distinct pattern corresponds to certain ranges of the three dimensionless material and geometrical parameters. Mechanical buckling might have provided a template for the morphology development in some fruits/plants that may confine and interact with certain biological processes such as cell growth and cell differentiation. Note that we employ the simplest spheroid model, and such a model could be refined to include the end/boundary (stem) constraints, anisotropic growth, and more sophisticated material/structural details, among others. Nevertheless, the encouraging results obtained through the self-assembled patterns of the model system show that the initiation and macroscopic topological characteristics of these patterns may be connected to mechanical principles, and the morphology of plants/fruits may be manipulated by the interaction between mechanical forces and biological processes.

Materials and Methods

To establish the model system in Cartesian coordinates, the spheroidal surface $(x^2 + y^2)/a^2 + z^2/b^2 = 1$ is created by rotating the ellipse, $x^2/a^2 + z^2/b^2 = 1$, about the z axis (vertical axis). The film thickness, t, is assumed to be much smaller than both a and b, and the film subtends a complete cover to the substrate. The film (in analogue to the fruit/vegetable shell) remains bonded to the substrate (core) throughout deformation. The growth is assumed to be isotropic within both film and substrate, but the unconstrained growth coefficient (expansion rate) is larger in the film. The mechanics of buckling is regulated by the minimization of system potential energy (because the film is bonded to the substrate, the substrate also deforms). Buckling simulation has been performed by using the finite element method (FEM). More details can be found in *SI Text*.

1. Bowden N, Brittain S, Evans AG, Hutchinson JW, Whitesides GM (1998) Spontaneous formation of ordered structures in thin films of metals supported on an elastomeric polymer. *Nature* 393:146–149.
2. Li C, Zhang X, Cao Z (2005) Triangular and Fibonacci number patterns driven by stress on core/shell microstructures. *Science* 309:909–911.
3. Mahadevan L, Rica S (2005) Self-organized origami. *Science* 307:1740.
4. Stafford CM, *et al.* (2004) A buckling-based metrology for measuring the elastic moduli of polymeric thin films. *Nat Mater* 3:545–550.
5. Pocivavsek L, *et al.* (2008) Stress and fold localization in thin elastic membranes. *Science* 320:912–916.
6. Kim D-H, *et al.* (2008) Stretchable and foldable silicon integrated circuits. *Science* 320:507–511.
7. Yoo PJ, Suh KY, Park SY, Lee HH (2002) Physical self-assembly of microstructures by anisotropic buckling. *Adv Mater* 14:1383–1387.
8. Chen X, Hutchinson JW (2004) A family of herringbone patterns in thin films. *Scripta Mater* 50:797–801.
9. Huang ZY, Hong W, Suo Z (2005) Nonlinear analyses of wrinkles in films on soft elastic substrates. *J Mech Phys Solids* 53:2101–2118.
10. Shipman PD, Newell AC (2004) Phyllotactic patterns on plants. *Phys Rev Lett* 92:168102.
11. Green PB (1999) Expression of pattern in plants: Combining molecular and calculus-based biophysical paradigms. *Am J Bot* 86:1059–1076.
12. Dumais J, Steele CR (2000) New evidence for the role of mechanical forces in the shoot apical meristem. *J Plant Growth Regul* 19:7–18.
13. Cosgrove DJ (2005) Growth of the plant cell wall. *Nat Rev Mol Cell Biol* 6:850–861.
14. Dumais J (2007) Can mechanics control pattern formation in plants? *Curr Opin Plant Biol* 10:58–62.
15. Steele CR (2000) Shell stability related to pattern formation in plants. *J Appl Mech* 67:237–247.
16. Priestley JH (1928) The meristematic tissues of the plant. *Ann Bot* 3:1–20.
17. Cao G, Chen X, Li C, Ji A, Cao Z (2008) Self-assembled triangular and labyrinth buckling patterns of thin films on spherical substrates. *Phys Rev Lett* 100:036102.
18. Chen X, Hutchinson JW (2004) Herringbone buckling patterns of compressed thin films on compliant substrates. *J Appl Mech* 71:597–603.
19. Audoly B, Boudaoud A (2008) Buckling of a stiff film bound to a compliant substrate—Part I: Formulation, linear stability of cylindrical patterns, secondary bifurcations pattern. *J Mech Phys Solids* 56:2401–2421.
20. Audoly B, Boudaoud A (2008) Buckling of a stiff film bound to a compliant substrate—Part II: A global scenario for the formation of herringbone pattern. *J Mech Phys Solids* 56:2422–2443.
21. Bargel H, Neinhus C (2005) Tomato fruit growth and ripening as related to the biomechanical properties of fruit skin and isolated cuticle. *J Exp Bot* 56:1049–1060.
22. Nath U, Crawford BCW, Carpenter R, Coen E (2003) Genetic control of surface curvature. *Science* 299:1404–1407.
23. Fleming AJ, McQueen-Mason S, Mandel T, Kuhlemeier C (1997) Induction of leaf primordia by the cell wall protein expansin. *Science* 276:1415–1418.
24. Sharon E, Marder M, Swinney HL (2004) Leaves, flowers and garbage bags: Making waves. *Am Sci* 92:254–261.
25. Darwin F (1897) *The Life and Letters of Charles Darwin: Including an Autobiographical Chapter* (Appleton, New York).

APPLIED PHYSICAL SCIENCES